THE JOURNAL OF BIOLOGICAL CHEMISTRY
Vol. 273, No. 2, Issue of January 9, pp. 964–973, 1998

Printed in U.S.A.

Water-soluble Nicotinic Acetylcholine Receptor Formed by α7 Subunit Extracellular Domains*

(Received for publication, August 4, 1997, and in revised form, October 6, 1997)

Gregg B. Wells‡§, René Anand¶‖, Fan Wang, and Jon Lindstrom**‡‡**

*From the ‡Department of Pathology and Laboratory Medicine, School of Medicine, University of Pennsylvania, Philadelphia, Pennsylvania 19104-6082, ¶Neuroscience Center of Excellence and Department of Biochemistry and Molecular Biology, Louisiana State University Medical Center, New Orleans, Louisiana 70112, and **Department of Neuroscience, School of Medicine, University of Pennsylvania, Philadelphia, Pennsylvania 19104-6074*

Water-soluble models of ligand-gated ion channels would be advantageous for structural studies. We investigated the suitability of three versions of the N-terminal extracellular domain (ECD) of the α7 subunit of the nicotinic acetylcholine receptor (AChR) family for this purpose by examining their ligand-binding and assembly properties. Two versions included the first transmembrane domain and were solubilized with detergent after expression in *Xenopus* oocytes. The third was truncated before the first transmembrane domain and was soluble without detergent. For all three, their equilibrium binding affinities for α-bungarotoxin, nicotine, and acetylcholine, combined with their velocity sedimentation profiles, were consistent with the formation of native-like AChRs. These characteristics imply that the α7 ECD can form a water-soluble AChR that is a model of the ECD of the full-length α7 AChR.

Nicotinic acetylcholine receptors (AChRs)[1] are integral-membrane, pentameric ion channels in the central and peripheral nervous systems that participate in signal transmission associated with the release of acetylcholine (ACh). A considerable collection of studies of their cell biology, electrophysiology, and structure makes them the best characterized family of a superfamily of homologous neurotransmitter-gated channels that includes glycine, γ-aminobutyric $acid_A$, and 5-hydroxytryptamine$_3$ receptors (1–3). Muscle-type AChRs are composed of four different subunits with the subunit composition $(\alpha1)_2(\beta1)\delta(\gamma \text{ or } \epsilon)$ and bind the snake venom toxin α-bungarotoxin (αBgt). Neuronal AChRs that do not bind αBgt are formed from combinations of α2, α3, α4, or α6 subunits with β2, β3, β4, and/or α5 subunits. Neuronal AChRs that do bind αBgt are formed from α7, α8, and α9 subunits, perhaps in combination with unknown subunits. When heterologously expressed, α7, α8, and α9 form functional homomeric AChRs that appear to contain five identical subunits.

AChRs are composed of five homologous membrane-spanning subunits that are ordered around a central, cation-selective channel. The topology of AChRs that is predicted by hydrophobicity plots has received substantial experimental support (4, 5). The approximately 200 residues at the N-terminal half of each AChR subunit are extracellular, are *N*-glycosylated, contain sites for agonist and antagonist binding, and form the vestibule through which cations reach the transmembrane channel. Relatively little of the remainder of the primary sequence is extracellular. Three of the four transmembrane domains (M1–M3) that form the channel are grouped together following the N-terminal extracellular domain (ECD) and are separated from M4 by a large cytoplasmic loop. For the muscle-type AChR, three distinct regions of the primary sequence around amino acid residues 86–93, 149, and 190–198 of α1 subunits and peptide loops around residues 34, 55–59, 113–119, and 174–180 of the γ or δ subunit contribute to the ACh binding sites at the interfaces between α and δ and between α and γ (or ε) subunits, based on photoaffinity labeling and site-directed mutagenesis (6, 7). Because of primary sequence and topological similarity, homologous residues at subunit-subunit interfaces in other neuronal AChR subunits are expected to have similar roles in the agonist binding site. For example, residues of the α7 subunit homologous to those of α1 and to those around γ55 and δ57 have been shown to contribute to the agonist binding in homomeric α7 AChRs (8, 9).

Our knowledge of the molecular structure of AChRs, however, is far from complete. Electron diffraction methods using two-dimensional, tubular arrays of AChRs from *Torpedo californica* have successfully yielded structural details at 9 Å resolution in three dimensions (10–12) and at 7.5 Å in two-dimensional projection (13). Achieving higher resolution, however, has been elusive with membrane-bound or detergent-solubilized AChRs. No member of this superfamily of integral-membrane receptors has been crystallized, and the intact AChRs are too large (more than 200 kDa) for nuclear magnetic resonance spectroscopy.

An AChR formed from the ECD may be a suitable structural model of a full-length AChR, if the ECD can both fold and oligomerize in the absence of the remainder of the subunit. Several lines of evidence suggest that the ECD meets these requirements. First, the specific interactions between subunits that are important in assembly of the muscle-type AChR and for formation of mature acetylcholine binding sites appear to depend primarily on the ECD (14–21). The long cytoplasmic loop of α1 participates in assembly subsequent to the formation of heterodimers (22). Second, membrane-tethered ECDs of

* This work was supported in part by a grant from the Pittsburgh Supercomputing Center through National Institutes of Health National Center for Research Resources Cooperative Agreement 2 p41 RR06009. The costs of publication of this article were defrayed in part by the payment of page charges. This article must therefore be hereby marked "*advertisement*" in accordance with 18 U.S.C. Section 1734 solely to indicate this fact.

§ Supported by National Institutes of Health Grant NS01903. To whom correspondence should be addressed: Dept. of Neuroscience, 235 Stemmler Hall, 36th and Hamilton Walk, University of Pennsylvania, Philadelphia, PA 19104-6074. Tel.: 215-573-2860; Fax: 215-573-2015; E-mail: wellsg@mail.med.upenn.edu.

‖ Supported by National Institutes of Health Grant NS33625.

‡‡ Supported by National Institutes of Health Grant NS11323 and by grants from the Muscular Dystrophy Association, Smokeless Tobacco Research Council, and Council for Tobacco Research-USA.

[1] The abbreviations used are: AChR, nicotinic acetylcholine receptor; ACh, acetylcholine; αBgt, α-bungarotoxin; ECD, extracellular domain; EK, enterokinase; ER, endoplasmic reticulum; GPI, glycophosphatidylinositol; M1–4, transmembrane domains 1–4; WS, water-soluble; mAb, monoclonal antibody; PBS, phosphate-buffered saline.

mouse muscle α1 and δ form heterodimers with ligand binding sites that reflect properties of a full-length AChR (23–25). Third, sequences of α7 that affect homomeric assembly also have been localized to the first half of the ECD and an area around M1 based on chimeras of α7 and α3 (26). According to this report, the long cytoplasmic loop of α7 is not essential for oligomerization.

To determine whether AChRs formed from the ECD (residues 1–208) of α7 subunits are water-soluble structural models for the ECD of the full-length α7 AChR, we expressed two constructs of the ECD of the α7 subunit with M1 retained and one construct of the ECD without M1 in *Xenopus* oocytes. The constructs with M1 were included to explore the feasibility of removing M1 by *in vitro* processing subsequent to *in vivo* synthesis. We examined ligand binding properties and velocity sedimentation profiles as indicators of global structure and local structure at the agonist binding site of the resulting AChRs, which we have designated as α7 ECD AChRs. We found that each construct, including the water-soluble one without M1, assembles into an AChR with affinities for ^{125}I-labeled αBgt (^{125}I-αBgt), nicotine, and ACh that match those of the full-length α7 AChR. These properties demonstrate that the α7 ECD forms a water-soluble α7 ECD AChR that can be a starting point for structural studies of this superfamily of ion channels.

EXPERIMENTAL PROCEDURES

Design of α7M1, α7 Enterokinase (α7EK), and α7 Water-soluble (α7WS) Plasmids—The full-length cDNA sequence of chicken α7 (27) previously was cloned into a modified SP64T expression vector (28, 29). For α7M1, which encodes the ECD of α7 up to the start of M2, the α7 coding sequence from the beginning of M2 to past the native stop codon was removed by digestion with *Bgl*II and *Bsm*I. It was replaced by a double-stranded oligonucleotide cassette coding in-frame for the 19-amino acid sequence SQVTGEVIFQTPLIKNPRV and a stop signal. This sequence contained the epitope of mAb 142 from residues 2 to 17 (5), followed by a *Mlu*I restriction site in the DNA sequence. The last native residue from α7 was Ile^{240}, according to the numbering scheme of the mature chicken α7 AChR subunit (27). The mAb 142 epitope was introduced for immunoblotting and for binding the subunit protein to mAb 142-coated plastic wells for solid-phase assays (5). The *Mlu*I site was included so that the epitope insert could be extended with additional residues after digestion with *Mlu*I and *Bsm*I. It has been shown that such extension may be necessary for accessibility of the epitope by the antibody (5).

The other construct that included M1 was α7EK, which was similar to α7M1 except for the inclusion of a peptide spacer between the end of the ECD and the beginning of M1. To prepare α7EK, a double-stranded oligonucleotide cassette coding for the 38-amino acid residue sequence TMRRRTGTVSISPESDRPDLSTFTSDDDDKILERRRTL was ligated in frame between the proximal *Bsm*AI and distal *Hga*I sites that are nearly juxtaposed to the 5′ side of M1 in α7M1. Residues 1–6 reconstructed the end of the N-terminal extracellular domain from residues Thr^{203} to Thr^{208}; the DNA sequence for residues 7–8 introduced a *Kpn*I site; residues 9–23 were the epitope for mAb 236 (5); the DNA sequence for residues 24–25 introduced a *Spe*I site; residues 26–31 (DDDDKI) were the specificity sequence for EK that is modeled after its site of proteolysis on trypsinogen (30, 31); the DNA sequence for residues 32–33 introduced a *Xho*I site; and residues 34–38 reconstructed the native sequence of Arg^{205} to Leu^{209} at the distal end of the insert. Beginning with Tyr^{210} (native numbering), the remainder of the sequence was identical to α7M1. The *Kpn*I, *Xho*I, and *Spe*I restriction sites were included so that the mAb 236 epitope and the target for protease digestion easily could be modified readily. A total of 27 amino acid residues were inserted between the proximal copy of Thr^{208} and the distal copy of Arg^{205}.

The third construct, α7WS, was truncated at the end of the ECD of α7 and did not include M1. To prepare α7WS, the full-length sequence of α7 was cut at the *Bgl*II site between M1 and M2. The resulting N-terminal domain sequence was cut at the *Bsm*AI site proximal to the start of the M1 coding sequence. A double-stranded oligonucleotide cassette coding for the 22-amino acid residue sequence TMRRRTQVTGEVIFQTPLIKNP followed by a stop codon was ligated between the *Bsm*AI site of the N-terminal sequence and the *Eco*RI site of a modified SP64T expression vector. Residues 1–6 of this sequence reconstructed the native sequence Arg^{203} to Thr^{208}; residues 7–22 constituted the epitope for mAb 142. The oligonucleotides were synthesized using the phosphoramidite method on a MilliGen oligonucleotide DNA synthesizer.

Protein Expression in Xenopus oocytes—DNA from each of the three plasmids was purified on a CsCl gradient. cRNA was synthesized using an SP6 mMessage mMachine™ kit (Ambion, Austin, TX) and linearized DNA. The cytoplasm of each oocyte was injected with approximately 50 ng of cRNA and incubated at 18 °C for 3–5 days in 50% Leibovitz's L-15 medium (Life Technologies, Inc.) in 10 mM HEPES, pH 7.5, containing 10 units/ml penicillin and 10 μg/ml streptomycin.

For α7M1 and α7EK, extraction of membrane-bound subunit protein with a buffer containing Triton X-100 was accomplished with a previously reported procedure (29). Oocytes were homogenized by hand in ice-cold buffer A (50 mM sodium phosphate, 50 mM NaCl, 5 mM EDTA, 5 mM EGTA, 5 mM benzamidine, 15 mM iodoacetamide, pH 7.5). The membrane-containing fraction was separated by centrifugation, was washed twice with buffer A, and then was extracted with buffer B (40 mM sodium phosphate, 40 mM NaCl, 4 mM EDTA, 4 mM EGTA, 4 mM benzamidine, 12 mM iodoacetamide, 2% Triton) during gentle agitation for 2 hours at 4 °C. The soluble fraction from this detergent extraction step was separated by centrifugation and was used for both Western blotting and assays of ligand binding.

For α7WS, the secreted fraction was defined as the subunit protein present in the L-15 medium incubating injected oocytes. Particulates in this fraction were removed by centrifugation. The cytoplasmic fraction of α7WS was defined as the subunit protein present in the soluble fraction following homogenization of the oocytes by hand in buffer A and centrifugation to sediment the insoluble, membranous component. The Triton-extracted fraction of α7WS was defined as the subunit protein present in the solvent following extraction in buffer B of the membranous component from the homogenization step during gentle agitation for 2 h at 4 °C.

Immunoblotting—Triton-extracted α7M1 and α7EK or secreted α7WS was incubated overnight at 4 °C with mAb 142 that had been coupled to Sepharose CL-4B (Pharmacia) with CNBr (32). After this concentration step, the protein was eluted at 55 °C with 2% SDS and 20 mM β-mercaptoethanol. Proteins were deglycosylated for 18 h at 37 °C with 1 unit of a mixture of endoglycosidase F and glycopeptidase F according to instructions of the manufacturer (Boehringer Mannheim). A sample without enzyme was run in parallel as the negative control.

Protein was denatured and reduced at 55 °C in SDS-polyacrylamide gel electrophoresis sample buffer containing 2% SDS, separated on a 13% acrylamide SDS-polyacrylamide gel electrophoresis gel, and transferred to an Immobilon-P polyvinylidene difluoride membrane (Millipore). After being blocked in 5% powdered milk in phosphate-buffered saline (PBS, 100 mM NaCl, 10 mM sodium phosphate, pH 7.5) containing 0.5% Triton, the membrane was incubated with 2 nM ^{125}I-mAb 142. Specific activities of the labeled antibodies ranged from 10^{17} to 10^{18} cpm/mol. Labeling was visualized by autoradiography.

Ligand Affinities—Immulon 4 plastic microwells (Dynatech Laboratories, Chantilly, VA) were coated with mAb 142 or mAb 236 for solid-phase assays (5). The wells were blocked with 3% bovine serum albumin in PBS. For α7M1 and α7EK, a volume of the Triton-solubilized protein from the equivalent of from one to three oocytes that had been injected with cRNA was added to each microwell. For the measurement of αBgt affinity, ^{125}I-αBgt was added to the Triton extract and incubated overnight at 4 °C. Total volume in each well was 100 μl. The wells were washed three times with ice-cold PBS containing 0.5% Triton, and the amount of radioactivity was measured using a γ counter. Each data point was measured in duplicate. For the competitive inhibition assays, the wells were washed free of the Triton solution after 24 h and loaded with ^{125}I-αBgt at 4 nM in the presence of L-nicotine or ACh. The wells were incubated 8 h at 4 °C before washing and then measuring the amount of radioactivity. Each data point was measured in duplicate. Nonspecific binding was measured with Triton-solubilized protein extracts from uninjected oocytes and generally was less than 5% of the specific binding.

For α7WS, the volume of L-15 medium above about six oocytes was added to mAb 142-coated microwells and incubated overnight at 4 °C for capture of the secreted α7WS. The L-15 was washed away with PBS. For the measurement of αBgt affinity in 0% Triton, ^{125}I-αBgt was added to buffer C (same composition as buffer B, except without Triton) and incubated overnight at 4 °C. Total volume in each well was 100 μl. The wells were washed three times with ice-cold PBS, and the amount of radioactivity was measured using a γ counter. Inhibition by nicotine and ACh in 0% Triton was measured after capture of the secreted α7WS, washing of L-15, and loading of each well with 0.6 nM ^{125}I-αBgt

and the appropriate amount of inhibitor in buffer C. Total volume in each well was 100 μl. The wells were incubated 8 h at 4 °C before washing and measuring the amount of radioactivity. Data points were measured in duplicate. Nonspecific binding was measured with L-15 medium that was used to incubate uninjected oocytes and generally was less than 10% of the specific binding. Buffer B was substituted for buffer C at the step of loading the wells with ^{125}I-αBgt or with ^{125}I-αBgt and nicotine or ACh for the ligand affinity measurements of α7WS in 2% Triton.

The equilibrium dissociation constants K_d for ^{125}I-αBgt were determined by least-squares, nonlinear fitting to a Hill-type equation (Equation 1) using the graphing software KaleidaGraph (Synergy Software)

$$C = C_0 \cdot \frac{1}{1 + \left(\frac{K_d}{L}\right)^n} \quad \text{(Eq. 1)}$$

where C is the measured signal (counts/min), C_0 is the maximal signal (which corresponds in this case to the maximum number of ^{125}I-αBgt binding sites), L is the concentration of ^{125}I-αBgt, n is the Hill coefficient. The half-maximal inhibition constants, IC_{50}, for nicotine and ACh in the presence of ^{125}I-αBgt were determined by nonlinear fitting to Equation 2, where L is the concentration of nicotine or ACh, C_0 is the maximal signal, and C_1 is a constant that represents signal that is not displaced by high concentrations of agonist. We used the Cheng-Prusoff equation (Equation 3) to estimate equilibrium dissociation constants from IC_{50} values (33),

$$C = C_0 \cdot \frac{1}{1 + \left(\frac{L}{IC_{50}}\right)^n} + C_1 \quad \text{(Eq. 2)}$$

$$K_d = \frac{IC_{50}}{1 + \frac{[\alpha\text{Bgt}]}{K_{d,\alpha\text{Bgt}}}} \quad \text{(Eq. 3)}$$

although other equations also have been described for that purpose (34). The K_d values shown in Table I are the average and standard error of at least three independent assays of ligand affinity unless otherwise noted. Uncertainties shown in figures are standard errors.

Sucrose Gradient Sedimentation—Membranes from 10–20 oocytes that had been injected with the α7M1, α7EK, or full-length α7 cRNA were extracted in buffer B. AChRs in membrane vesicles from *T. californica* and AChRs from the TE671 cell line (35) were solubilized in buffer B. About 200-μl aliquots of solubilized protein containing from 20 to 100 fmol of ^{125}I-αBgt binding sites were layered onto 5-ml sucrose gradients (5–20% (w/v)) in 0.5% Triton solution of 100 mM NaCl, 10 mM sodium phosphate, 5 mM EGTA, 5 mM EDTA, and 1 mM NaN_3 at pH 7.5. The gradients were centrifuged 75 min at 70,000 rpm (approximately 340,000 × *g*) and 4 °C in a Beckman NVT90 rotor. For determining a ligand binding profile, aliquots of 11 drops each (approximately 130 μl) from the gradient were collected into Immulon 4 plastic microwells coated with mAb 142 for α7M1, mAb 236 for α7EK, or mAb 318 (a rat monoclonal antibody against an epitope in the cytoplasmic domain) (27) for the full-length α7. The entire gradient was collected in 40 fractions. After 24 h at 4 °C, the microwells were washed and filled with from 4 to 12 nM ^{125}I-αBgt in buffer B for 6 h at 4 °C, followed by washing and quantitation of bound ^{125}I-αBgt by γ counting.

Processing of α7WS was slightly more involved because of the low concentration of the secreted protein in the incubation medium. The protein was concentrated by binding overnight at 4 °C to α-toxin that had been isolated from the venom of *Naja naja siamensis* with ion exchange chromatography (36) and then coupled to Sepharose CL-4B with CNBr (32). The bound protein was eluted from the α-toxin with 200 μl of 100 mM nicotine and was layered onto 5-ml sucrose gradients (5–20%) without Triton in centrifuge tubes. The gradient was centrifuged 75 min at 70,000 rpm (approximately 340,000 × *g*) and 4 °C, as was done for α7M1 and α7EK. The entire gradient was collected in 39 fractions of 6 drops each, because the drop size was larger in the absence of detergent. After 24 h at 4 °C, the microwells were washed and filled with 1 nM ^{125}I-αBgt in buffer C for 6 h at 4 °C, followed by washing and quantitation of bound ^{125}I-αBgt by γ counting.

Comparison of AChR Yields—The yield was defined as the theoretical maximal amount of bound ^{125}I-αBgt, which was the value of C_0 in Equation 1 from ^{125}I-αBgt-binding assays. The AChR yield was calculated in terms of ^{125}I-αBgt binding sites per oocyte.

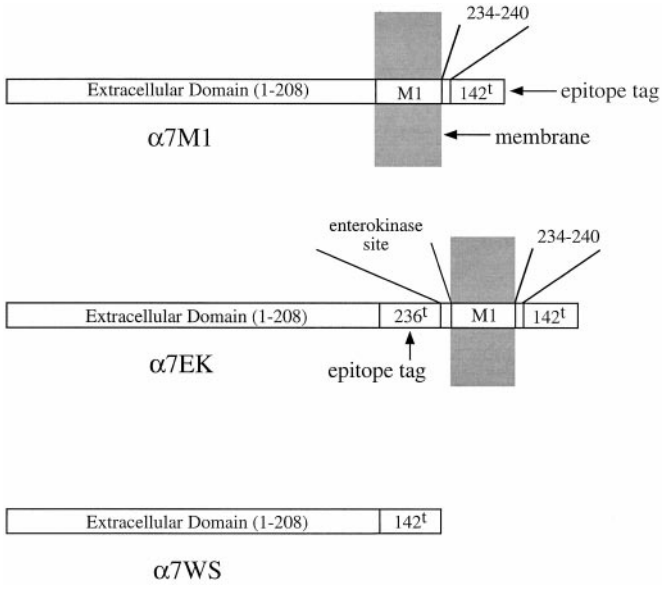

FIG. 1. **Designs of the three α7 ECD subunit proteins α7M1, α7EK, and α7WS.** The ECD, which extends from residues 1 to 208 of the mature chicken α7 AChR (27) is included in each protein. In α7M1 and α7EK, the first transmembrane domain, M1, extends from residues 209 to 233. The α7 sequence from residues 234 to 240, which extends to the beginning of M2, is included after M1 in these two proteins. The segment labeled *142t* on the C-terminal side of M1 is the epitope tag for mAb 142. Besides the mAb 142 epitope, α7EK also contains an epitope tag for mAb 236, designated *236t*, as well as an EK-specific protease site between the extracellular domain and M1. In contrast to the two membrane-tethered proteins, α7WS does not contain M1; the mAb 142 epitope tag of the α7WS protein follows directly after the ECD.

RESULTS

Expression of α7 ECD Proteins in Xenopus Oocytes—The three variations of the ECD sequence of the α7 subunit were studied (Fig. 1). The first construct, α7M1, includes the N-terminal ECD, M1, and the portion of α7 between M1 and M2 up to residue Ile^{240}. It was intended to demonstrate the pharmacological properties and oligomerization behavior of the α7 subunit proximal to M2 and tethered to the membrane through M1. The second construct, designated α7EK, contains a peptide spacer of 27 amino acid residues that is spliced between Thr^{208} and Leu^{209} at the junction of the ECD and M1. α7EK also contains M1 and terminates at Ile^{240}, like α7M1. The position of an RRR motif from 205 to 207 at the junction of the ECD with M1 suggests a structural role for these positively-charge residues; therefore, the native sequence Arg^{205} to Thr^{208} was repeated at the C-terminal end of the interposed segment before M1. The name "α7EK" is derived from the DDDDKI sequence that was included in the peptide spacer for site-specific proteolysis by EK. α7EK was intended to test the feasibility of removing M1 from the ECD by *in vitro* enzymatic proteolysis after synthesis. The third variation, α7WS, was intended to be a direct route to a water-soluble α7 ECD AChR. It is truncated at Thr^{208}, just before M1 and contains no transmembrane domain. Epitopes for monoclonal antibodies mAb 142 and mAb 236 were included in the truncated constructs so that the proteins could be detected by immunoblotting and tethered through the antibodies to plastic wells for solid-phase ligand-binding assays (5).

Immunoblotting of Triton X-100 extracts from oocytes injected with α7M1 and α7EK cRNA confirmed the expression of these proteins (Fig. 2). α7M1 before deglycosylation migrated at an apparent mass of 37 kDa; α7EK migrated at 40 kDa. These apparent masses were about 7 kDa higher than the values of 30 kDa for α7M1 and 33.5 kDa for α7EK that were

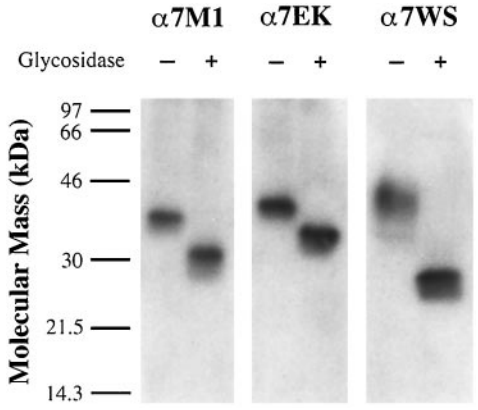

FIG. 2. **Protein expression and glycosylation of α7M1, α7EK, and α7WS demonstrated by immunoblotting with ^{125}I-mAb 142.** Deglycosylated protein is compared with control protein that was processed in parallel except without glycosidase. The presence (+) or absence (−) of glycosidase is noted *above* each lane. Each lane of α7M1 and α7EK contains the protein from about two oocytes; each lane of α7WS contains the protein secreted from about 24 oocytes. Although α7WS has the lowest molecular weight as calculated from amino acid sequences, it is the most heavily glycosylated and migrates at the largest apparent molecular weight. Triton extracts and incubation medium from uninjected oocytes were used as negative controls and showed no binding of ^{125}I-mAb142. The positions of molecular mass markers are indicated on the *left*.

calculated from amino acid compositions. The detection of predominately a single band before deglycosylation suggested that post-translational modifications were comparatively uniform on all molecules. Deglycosylation shifted each band to approximately the molecular mass of the protein calculated without modifications.

Without M1, α7WS was secreted in soluble form into the incubation medium by oocytes that had been injected with α7WS cRNA. The secreted protein displayed an apparent mass of about 41 kDa by immunoblotting, compared with a calculated mass of 26 kDa (Fig. 2). The detection of a diffuse pattern of bands before deglycosylation suggested more heterogeneous glycosylation than was present on α7M1 and α7EK. Deglycosylation shifted the apparent mass down to about 26 kDa, confirming that α7WS had the most extensive glycosylation of the three proteins. The larger shift in apparent mass compared with α7M1 and α7EK also suggested that the pattern of glycosylation differed between membrane-tethered and soluble forms of the ECD. An additional observation from the immunoblot is that the yield of secreted α7WS was about 10-fold less than the yields of α7M1 and α7EK from Triton-solubilized membrane fractions, based on a comparison of the numbers of injected oocytes needed to produce approximately equal signals on the immunoblot.

High Affinity Binding of ^{125}I-αBgt to α7 ECD AChRs—Because high affinity binding of αBgt is a hallmark of the α7 AChR, measurements of binding affinity with ^{125}I-αBgt were appropriate starting points for analyzing the functional and structural properties of the three α7 ECD constructs. The equilibrium dissociation constant, K_d, of ^{125}I-αBgt was 1.6 nM for α7M1 and 1.9 nM for α7EK when measured in solid phase assays in which the Triton-solubilized proteins were bound in mAb 142-coated wells (Fig. 3 and Table I). These values compare favorably with the published K_d of 1.6 nM for ^{125}I-αBgt binding to Triton-solubilized full-length α7 AChR and for α7-containing AChR from chick brain (37). Binding of ^{125}I-αBgt was measured for α7EK by also using the mAb 236 epitope tag to bind the protein to mAb 236-coated wells. The K_d was 2.3 nM, demonstrating that the mAb 236 epitope tag at the C-terminal end of the ECD did not interfere significantly with the function

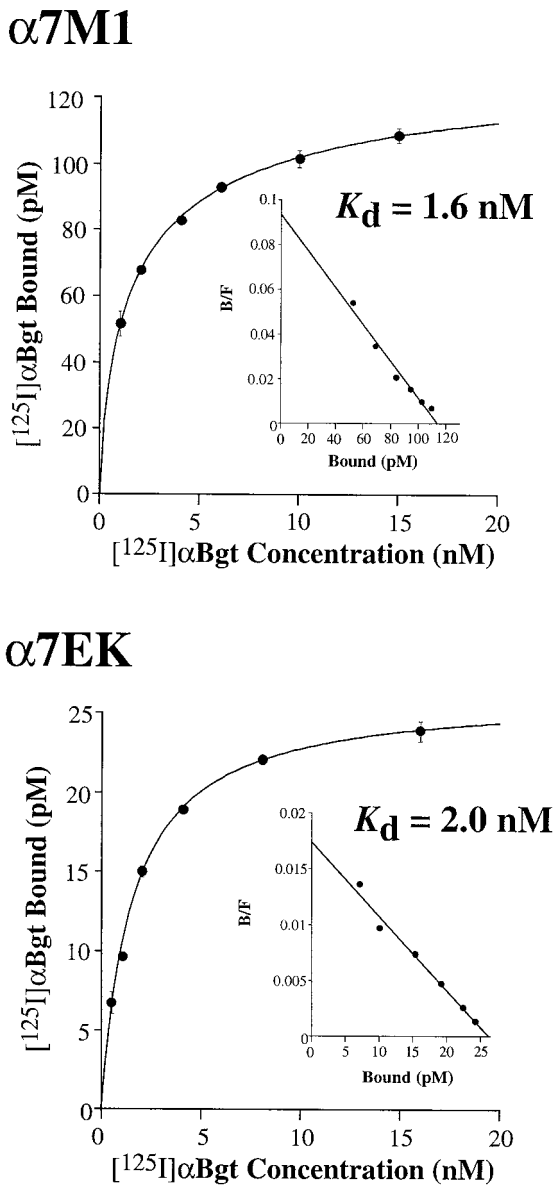

FIG. 3. **Equilibrium binding of ^{125}I-αBgt to α7M1 and α7EK AChRs.** The Triton-solubilized AChRs were bound to mAb 142-coated microwells. Assays were performed in 2% Triton X-100. The curves are the best fits of Equation 1 to the data. Each data point is the mean of duplicate determinations. Scatchard analysis of the data is shown in the *insets*. The K_d values are taken from Table I. Data from representative single experiments are shown.

of the αBgt binding site.

The affinity of secreted α7WS for ^{125}I-αBgt was measured first without Triton (Fig. 4 and Table I). The K_d value of 0.4 nM was about 4-fold smaller than the values for Triton-solubilized α7M1, α7EK, and full-length α7. The presence of 2% Triton during the binding assay of α7WS for ^{125}I-αBgt increased the value of K_d to 1.7 ± 0.1 nM (Fig. 4), which is in the range measured for the Triton-solubilized AChRs. Triton, however, did not significantly affect the total number of ^{125}I-αBgt binding sites. The ratio of the number of binding sites calculated from Equation 1 in the absence of Triton compared with the number of binding sites in the presence of Triton from otherwise identical pools of secreted α7WS was 0.99 ± 0.13 (n = 2). Only the secreted fraction of α7WS bound ^{125}I-αBgt to a measurable extent, despite the significant amount of α7WS protein that was retained intracellularly. The total amount of α7WS protein per oocyte that was detected in the cytoplasmic and the

TABLE I
Ligand affinities for full-length α7 and α7 ECD AChRs

AChR	Ligand affinity (K_d)					
	αBgt	n^a	Nicotine	n	ACh	n
			μM			
α7 AChR (full-length)[b]	0.0016 ± 0.0001		0.54 ± 0.02		25 ± 4.7	
α7-containing AChRs from chick brain[b]	0.0017 ± 0.0001		1.4 ± 0.2		100 ± 10	
α7M1 AChR	0.0016 ± 0.0001	0.7 ± 0.1	1.0 ± 0.4[c]	1.2 ± 0.1	50 ± 20[c]	1.2 ± 0.4
α7EK AChR						
mAb 142 tether for assay	0.0020 ± 0.0004	0.8 ± 0.1	1.0 ± 0.3[c]	1.7 ± 0.2	50 ± 20	1.3 ± 0.2
mAb 236 tether for assay	0.0029 ± 0.0006	0.8 ± 0.1	1.4 ± 0.7	1.1 ± 0.2	60 ± 30	1.1 ± 0.1
α7WS AChR						
In 0% Triton X-100	0.0004 ± 0.0001	1.3 ± 0.1	0.09 ± 0.05	1.6 ± 0.1	1.3 ± 0.4	1.6 ± 0.3
In 2% Triton X-100	0.0017 ± 0.0001[c]	1.1 ± 0.1	0.22 ± 0.01	1.7 ± 0.1	3.9 ± 0.3	2.0 ± 0.1

[a] Hill coefficient n from Equations 1 or 2.
[b] Data from α7 AChRs expressed in oocytes and solubilized in Triton X-100 (37).
[c] Values determined from two independent measurements of IC_{50}. All other values were determined from three or more independent measurements.

Triton-solubilized membrane fractions by immunoblotting was approximately equal to the amount of Triton-solubilized α7M1 or α7EK protein in similarly-injected oocytes. Hence all three constructs apparently were synthesized and accumulated to an approximately equal extent. The intracellular pool of α7WS, however, showed no significant binding of ^{125}I-αBgt.

The yield of ^{125}I-αBgt binding sites from each of the three ECD proteins was measured by the binding of ^{125}I-αBgt to AChR on mAb 142-coated wells (Fig. 5). These measurements assumed that the mAb 142 epitope in each protein was equally accessible to the antibody. The yield of 8 ± 1 fmol of ^{125}I-αBgt binding sites per oocyte with α7M1 AChR was the largest among the three proteins. This value is near the value of 15 fmol per oocyte that was reported for Triton-solubilized AChR from the full-length α7 subunit expressed in oocytes (29). Compared with α7M1, the addition of the peptide spacer in α7EK decreased the yield of AChR by about three-quarters to 1.9 ± 0.6 fmol of ^{125}I-αBgt binding sites per oocyte. The yield of secreted α7WS AChR was the smallest of the three at 0.21 ± 0.02 fmol of ^{125}I-αBgt binding sites per oocyte. These comparisons indicate that insertion of residues before M1 or the absence of M1 decreases the yield of ECD AChRs.

High affinity for ^{125}I-αBgt was the first step in demonstrating the structural similarity of α7M1, α7EK, and α7WS AChRs to the full-length α7 AChR. It was only an initial test of the properties that we hoped to find in a model AChR. Specifically, we were seeking a model that also was a pentamer and that had native-like affinity for agonists like nicotine and ACh. High affinity for αBgt does not necessarily imply either of these properties. Muscle-type AChR illustrates this point. The human α1 subunit in the absence of other muscle-type subunits binds αBgt relatively tightly, with K_d of 0.6 nM compared with K_d of the pentameric muscle-type AChR of 0.1 nM (35). Instead of a pentamer, however, it exists as a monomer according to its velocity sedimentation profile relative to the profiles of fully assembled muscle-type AChR and αδ and αγ dimers (38, 39). Moreover, it does not bind agonists with native-like affinity. In light of these characteristics for α1, other experiments besides binding of ^{125}I-αBgt were required for assessing the oligomerization of the α7 ECD constructs.

Velocity Sedimentation Implies α7M1, α7EK, and α7WS Form Multimeric AChRs, Probably Pentamers—Oligomerization of α7M1, α7EK, and α7WS proteins was examined first with velocity sedimentation profiles in sucrose gradients. The proteins were detected by binding of ^{125}I-αBgt in solid-phase assays. These profiles were compared with full-length AChRs and monomeric α1 subunits as sedimentation standards. Fully assembled, full-length α7 AChR (calculated molecular mass of 272 kDa from amino acid sequence) were pentameric standards (37). Muscle-type AChR from *T. californica* were pentameric (*i.e.* a monomeric AChR with calculated molecular mass of 268 kDa) and decameric standards (*i.e.* a dimeric AChR with calculated molecular mass 536 kDa) (40). The monomeric α1 subunit (calculated molecular mass of 52 kDa) from the human rhabdomyosarcoma cell line TE671 was the monomeric standard (35). As expected because of their much larger molecular masses, the pentameric AChR standards sedimented faster than monomeric α1 subunit (Fig. 6).

The single ^{125}I-αBgt binding peak from α7M1 and from α7EK also sedimented much faster than the monomeric α1 subunit and slightly slower than the full-length AChRs (Fig. 6). Two conclusions can be drawn from these velocity sedimentation data in the absence of measurements of diffusion and partial specific volume. First, the position of the ^{125}I-αBgt binding peak was distant from the α1 monomer standard, strongly suggesting that a multimeric species was responsible for the ^{125}I-αBgt binding. Second, this multimeric species probably was a pentamer. This conclusion about subunit stoichiometry was deduced from both the single peak and its relatively narrow distribution. The single peak implied that a multimer with a single distinct stoichiometry was the dominant species that bound ^{125}I-αBgt with nanomolar affinity. In contrast, if multiple stoichiometries such as dimers and trimers and tetramers had significant representation in the high affinity population, then one would have expected either several discrete peaks or a low, broad profile. Because of the pentameric structure of the full-length α7 AChR (41), the most likely stoichiometry for α7M1 and α7EK AChRs also was pentameric, although minor fractions of smaller oligomers may also have been present. Moreover, it has been reported that only pentameric α7 subunits bind ^{125}I-αBgt with nanomolar affinity, whereas monomeric full-length subunits and aggregated or incompletely assembled forms do not (37).

Velocity sedimentation of the secreted α7WS in sucrose gradients also revealed a single ^{125}I-αBgt binding peak (Fig. 6). It sedimented slightly slower than the peaks for α7M1 and α7EK. As with α7M1 and α7EK, the position of the single, relatively narrow peak that was distant from the peak of the α1 subunit did not suggest a monomeric form for α7WS AChR and was consistent with the conclusion that the dominant form of α7WS AChR was a pentamer.

High Affinity Binding of Nicotine and ACh to α7 ECD AChRs—High affinity binding for agonists was the second test of oligomerization and the last test of structural equivalence between the α7 ECD AChRs and the full-length α7 AChR. Interpretation of this test was based on an analogy with characteristics of the α1 subunit of the muscle-type AChR. High affinity for agonists develops for α1 only after it assembles with

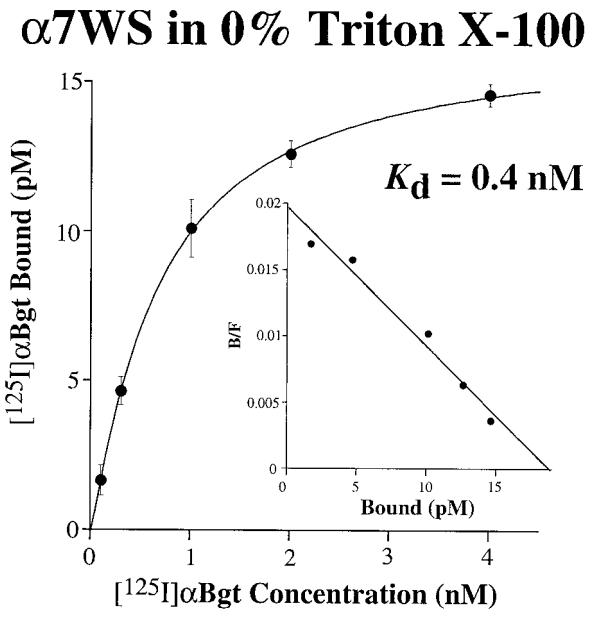

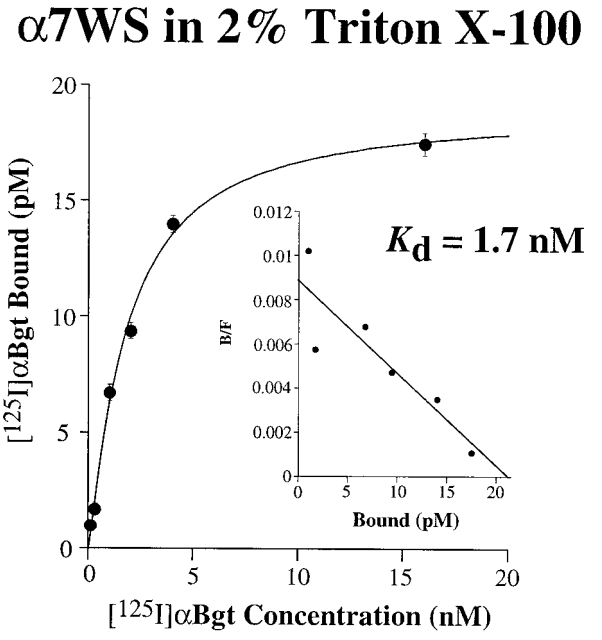

FIG. 4. **Effect of Triton X-100 on the equilibrium binding of ^{125}I-αBgt to α7WS.** α7WS was bound to mAb 142-coated microwells. The binding assays with ^{125}I-αBgt were performed without Triton X-100 (*upper panel*) or with 2% Triton X-100 (*lower panel*). The curves are the best fits of Equation 1 to the data. Each data point is the mean of duplicate determinations. Scatchard analysis of the data is shown in the *insets*. The K_d values are taken from Table I. In the absence of Triton, K_d was about 4-fold smaller than the values measured for α7M1 and α7EK. In the presence of Triton, however, the value for α7WS shifted into the range for the M1-containing AChRs. Data from representative single experiments are shown.

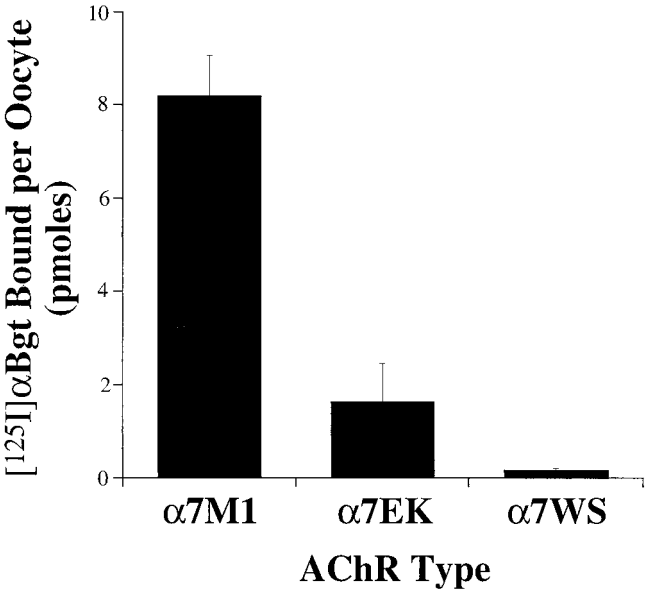

FIG. 5. **Comparison of yields of α7 ECD AChRs from α7M1, α7EK, and α7WS.** The yield was defined as the number of ^{125}I-αBgt binding sites per oocyte. This value was the maximal amount of bound ^{125}I-αBgt that was estimated from solid phase binding assays on mAb 142-coated microwells using Equation 1 (calculated from the value of C_0). At least three independent measurements were performed for each type of AChR. From 20 to 50 oocytes were pooled for the assays of α7M1 and α7EK. The incubation medium from 80 to 160 oocytes was the source of AChRs for the assays of α7WS.

δ or γ (39, 42), because the agonist binding site consists of structural components from both subunits at αδ and αγ interfaces (3). Similarly, if α7M1, α7EK, and α7WS AChRs indeed were pentamers and structural models of the full-length α7 AChR, then we expected native-like affinities for nicotine and ACh.

The affinities of α7M1 and α7EK for the small ligands nicotine and ACh were measured by competitive inhibition of the binding of ^{125}I-αBgt (Fig. 7 and Table I). The equilibrium dissociation constants, K_d, of α7M1 and α7EK were 1.0 μM for nicotine and 50 μM for ACh. In the case of α7EK, tethering in the solid phase assays via the mAb236 epitope tag slightly increased the values of K_d for nicotine and ACh to 1.4 μM and 60 μM, respectively. For both proteins, the K_d values are similar to those for Triton-solubilized, full-length α7 and for α7-containing AChRs from chick brain (Table I). Competitive binding with each ligand eliminated almost all binding of ^{125}I-αBgt, implying that the majority of the ^{125}I-αBgt binding sites also bound nicotine and ACh.

In inhibition assays with ^{125}I-αBgt and α7WS, the values of K_d for nicotine binding in the absence of Triton were 10-fold smaller than the values for nicotine binding to α7M1 and α7EK in the presence of Triton (Fig. 8 and Table I). The values for ACh binding to α7WS without Triton were 40-fold smaller than the values for ACh binding to α7M1 and α7EK with Triton. The water-soluble α7WS AChR without Triton, therefore, bound to small ligands more tightly than did the full-length α7 AChR in Triton. The presence of 2% Triton in the inhibition assays increased the values of K_d by about 3-fold (Fig. 8). As with α7M1 and α7EK, the majority of the ^{125}I-αBgt binding sites of α7WS AChR also bound nicotine and ACh, as shown by the elimination of almost all binding of ^{125}I-αBgt at high concentrations of agonists in either the presence or absence of Triton.

In light of the velocity sedimentation data, these results confirm that the α7M1, α7EK, and α7WS AChRs are oligomers and probably are pentamers. These results demonstrate that the α7 ECD with or without M1 is sufficient for the expression of a α7 ECD AChR with native-like affinities for αBgt and nicotinic agonists.

DISCUSSION

Structural Implications of the Ligand Binding Properties and Oligomerization of ECD AChRs—We have shown that the N-terminal ECD of the α7 AChR subunit with or without M1 forms an AChR whose ligand-binding and sedimentation prop-

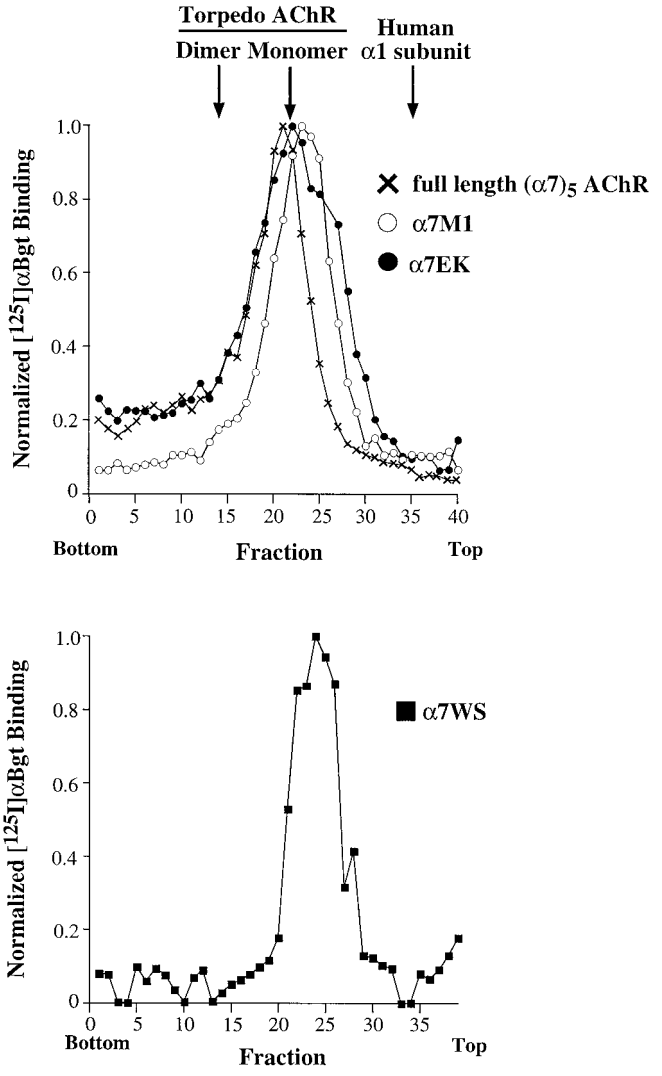

FIG. 6. **Velocity sedimentation profiles of α7 ECD AChRs and full-length α7 AChRs.** The profiles of ^{125}I-αBgt binding to full-length α7 AChR, α7M1 AChR, and α7EK AChR that were sedimented on a 5–20% sucrose gradient with 0.5% Triton X-100 are shown in the *upper panel*. Two of the *arrows* indicate the peaks of ^{125}I-αBgt binding to *Torpedo* AChR monomers (five subunits) and dimers (10 subunits) (40) that were observed in a parallel experiment. The peak of ^{125}I-αBgt binding to the human α1 monomeric subunit from the TE671 cell line from a parallel experiment is indicated by a third *arrow*. These three proteins served as oligomerization standards for the α7 ECD AChRs. The profiles for α7M1 and α7EK are inconsistent with monomers as the high affinity species but are consistent with pentamers. The *lower panel* shows the profile of the α7WS AChR on a 5–20% sucrose gradient without Triton. The profile again is inconsistent with a monomer as the high affinity species but is consistent with a pentamer.

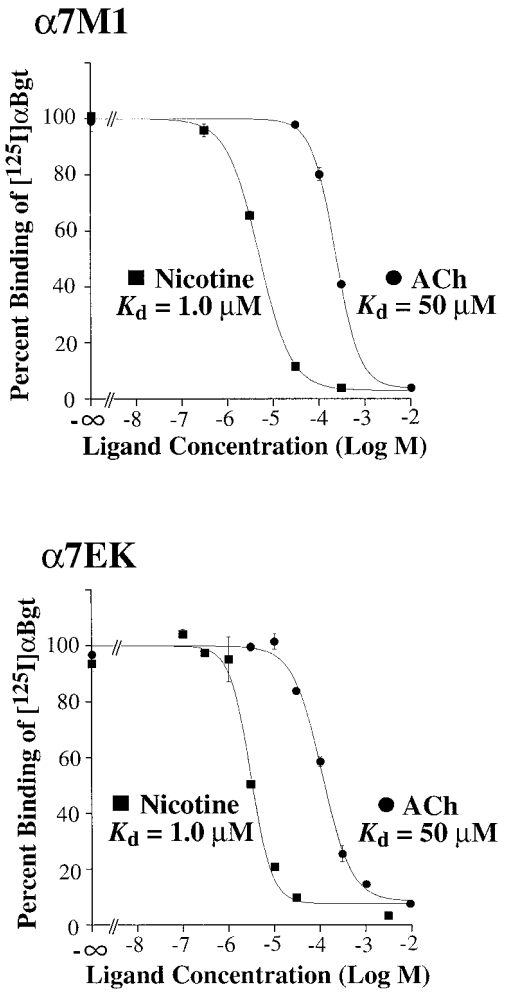

FIG. 7. **Competitive inhibition by nicotine and ACh of ^{125}I-αBgt binding to Triton-solubilized α7M1 and α7EK AChRs.** The AChRs first were bound to mAb 142-coated microwells. After washing, the microwells were loaded with 4 nM ^{125}I-αBgt in 2% Triton X-100 and varying concentrations of either nicotine or ACh. The curves are the best fits of Equation 2 to the data. Each data point is the mean of duplicate determinations. K_d values are taken from Table I. Similar inhibition assays were performed with α7EK using mAb 236-coated microwells (Table I). Data from representative single experiments are shown.

erties imply that it is a structural model of the full-length AChR. In particular, the α7WS AChR is water-soluble. The ECD, therefore, constitutes an autonomous unit capable of folding and assembling in the absence of the transmembrane, cytoplasmic, and other extracellular portions of the α7 subunit sequence. We examined three characteristics that implied retention of the native-like structure in the three ECD AChRs: 1) high affinity binding of αBgt, which is a hallmark of α7 AChRs; 2) velocity sedimentation, which is most consistent with assembly of each of the three α7 ECD subunits into pentamers; and 3) native-like affinities for nicotine and ACh.

First, the affinity for ^{125}I-αBgt of each of the three α7 ECD AChRs was equal to or higher than that of the fully assembled, full-length α7 AChR. Because the αBgt binding site incorporates noncontiguous regions of primary sequence, these affinities suggest that the global structure of each α7 ECD AChR models the structure of the ECD in the full-length α7 AChR. The moderately higher affinity of the α7WS AChR for ^{125}I-αBgt reverted back into the range of K_d values observed with α7M1 and α7EK AChRs when Triton was included in the assay. Triton could have exerted its effects by modifying the interaction of αBgt with either the AChR or with the solvent environment, since both interactions can affect K_d. In other words, Triton may have caused structural perturbations of the AChR that affected the binding site, or ^{125}I-αBgt may have partitioned differently in Triton-containing solvent compared with detergent-free solvent.

Second, velocity sedimentation data suggested that the α7 ECD subunits had assembled into multimers that probably were pentamers. Other AChRs or AChR subunits were used as oligomerization standards for estimating the extent of oligomerization of the α7 ECD subunits. The single ^{125}I-αBgt binding peak for each of the ECD AChRs migrated on the sucrose gradient slightly slower than full-length, pentameric α7 AChR and *Torpedo* AChR and much faster than the peak of monomeric α1 subunit. Although differences in the amount of

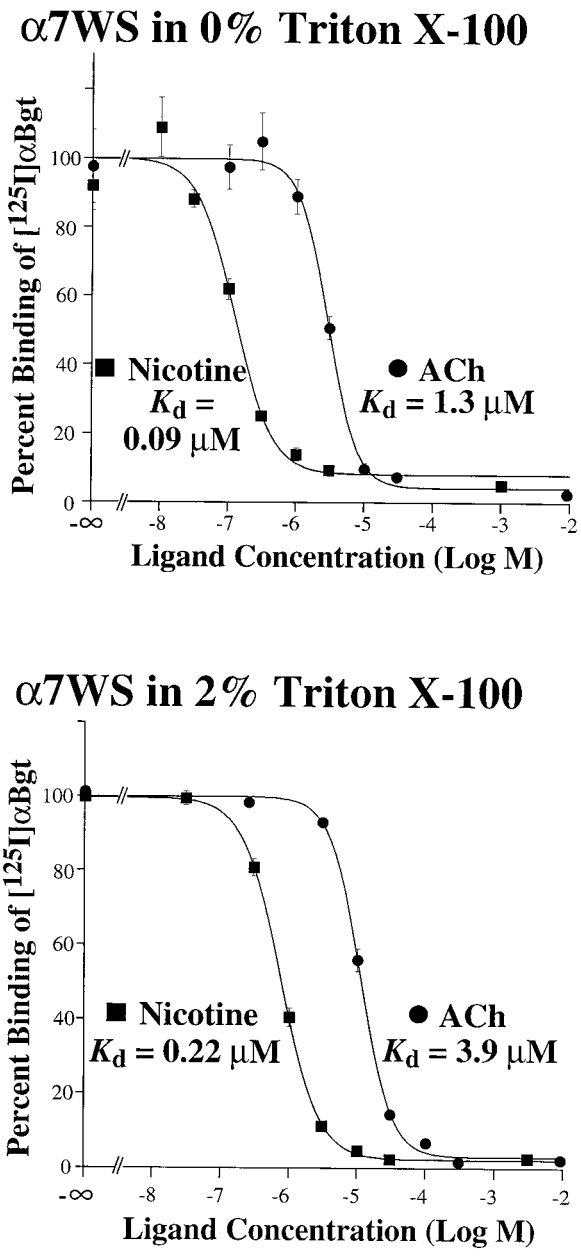

FIG. 8. **Effect of Triton X-100 on the inhibition by nicotine and ACh of ^{125}I-αBgt binding to α7WS AChR.** The α7WS AChR first was bound to mAb 142-coated microwells in the absence of Triton X-100. After washing, the microwells were loaded with a fixed concentration of ^{125}I-αBgt (0.6 nM with 0% Triton or 4 nM with 2% Triton) and with varying concentrations of either nicotine or ACh. The curves are the best fits of Equation 2 to the data. Each data point is the mean of duplicate determinations. K_d values are taken from Table I. Data from representative single experiments are shown.

bound detergent (40) and in molecular shape (43, 44) will affect the sedimentation of AChRs, we do not think that these effects alone can account for the differences between the position of the monomeric subunit standard and the positions of α7 ECD AChRs on the gradients. A reasonable interpretation of the position of the ^{125}I-αBgt binding peaks relative to the monomeric α1 subunit peak was that these α7 ECD subunits were not monomeric. Multimeric stoichiometry also is consistent with their native-like affinity for agonists. Given that full-length α7 AChR are pentamers (41), the single, relatively narrow ^{125}I-αBgt binding peak from each α7 ECD AChR probably arose from pentamers.

Third, affinities of the three α7 ECD AChRs for nicotine and ACh also matched or were slightly higher than those of the full-length α7 AChR. In the case of α7WS AChR, Triton reduced the affinity of nicotine and ACh compared with that observed without Triton. The differences in affinity for agonists of α7WS AChR compared with α7M1 and α7EK AChRs were not caused solely by Triton and may have been contributed in part by M1. Overall, these results imply that the local structure of the ACh binding site of each of the α7 ECD AChRs closely matches that of the full-length α7 AChR. By analogy with the behavior of the muscle-type AChR (39, 42), the binding site for small ligands is thought to form at interfaces between subunits. Therefore, native-like affinities for agonists by the α7 ECD AChRs, combined with the results from velocity sedimentation, confirmed that the α7 ECD subunits had assembled into multimers.

The α7EK subunit demonstrated another structural property of the ECD AChRs. Splicing a peptide spacer of 27 amino acid residues between these two domains did not significantly alter ligand affinity. Therefore, strict continuity of the native primary amino acid sequence between the ECD and M1 is not required for formation of the agonist binding site or for oligomerization. In other words, an ECD that is displaced away from M1 by a peptide spacer retains its assembly and binding properties. This flexibility in design raises the possibility of first expressing a membrane-bound ECD AChR, followed by release of a water-soluble ECD AChR from M1 by enzymatic proteolysis *in vitro*.

Elimination of transmembrane domains either by recombinant techniques or by proteolysis of native protein has been the starting point for structural studies of other integral membrane proteins. In the family of ionotropic glutamate receptors, the soluble agonist binding domain of GluR-B and GluR-D was successfully designed by fusion of discontinuous sections of the primary sequence that apparently are separated by two transmembrane domains (45, 46). This strategy also has been successful for the x-ray crystallography of many integral membrane proteins including growth hormone receptor (47), prolactin receptor (48), tissue factor (49), interferon-γ receptor (50), human class II histocompatibility antigen (51), insulin receptor protein-tyrosine kinase domain (52), α and β chains of the T cell receptor (53, 54), neuraminidase (55), hemagglutinin (56), and bacterial aspartate receptor (57).

Yield of ECD AChRs—The protein sequence between the beginning of M1 and the start of M2 (residues Leu^{209} to Ile^{240}) was needed for production of AChRs from the ECD at a level comparable to that of the full-length AChR. M1 probably was the key component of this region. Compared with the yield of AChRs from α7M1 AChR, the yield was smaller from α7EK and even smaller from α7WS. The differences were unlikely to be caused by reduced translation efficiencies of α7EK and α7WS, because of the extent of sequence identity among all three designs and because the amounts α7EK and intracellular α7WS proteins per oocyte that were detected by immunoblotting were approximately equal to the amount of α7M1. Instead, the difference in the case of α7EK AChR suggests some adverse effects on folding and assembly caused by the alteration of the primary sequence at the ECD/membrane interface.

The low yield in the case of α7WS AChR highlighted an important role for M1. M1 has been shown to function as a tether to the ER membrane during the dimerization of truncated α1 and δ subunits in the ER (23). It was successfully replaced in mouse α1 by unrelated transmembrane domains with unrelated primary sequences or with a glycosylphosphatidylinositol (GPI) moiety (24). A similar role for M1 probably applies to the production of α7 ECD AChRs. M1 constrains the subunits to a membrane surface, which may favor orientations

between subunits that are required for assembly and may help retain them in the endoplasmic reticulum (ER) and Golgi apparatus for folding, subunit assembly, and post-translational modifications. In contrast, failure to retain the subunits on the ER and Golgi membranes removes such constraints and decreases the efficiency of these processes. In particular, M1 may enhance folding and assembly by increasing the local concentration of subunits relative to folding cofactors, such as calnexin, that are found in the ER membrane (58, 59).

Attaching the ECD to a membrane may not be the sole function of M1 for α7M1 and α7EK, however. Instead, the yield of AChRs may depend on particular properties of M1. Chimeras of α7/α3 (26) and point mutations in M1 of α7 (60) demonstrate that the specific sequence used in the first transmembrane domain affects the yield of surface AChRs. Similarly, the total amount of bound ^{125}I-αBgt per oocyte varied when unrelated transmembrane domains replaced any one of the regions M1–M4 of α1 in recombinantly expressed *Torpedo* AChRs (61).

Strategy for Structural Studies of α7 ECD AChRs—What is the optimum design of an α7 ECD AChR for structural studies? The complete ECD of the α7 subunit incorporating all of the amino acid sequence up to the start of M1 probably is necessary to satisfactorily reproduce the ligand-binding and assembly properties of the full-length α7 AChR. Although we did not attempt to truncate the α7 ECD N-terminal to Thr^{208}, results from the mouse α1 subunit suggest that there is little flexibility for moving the truncation point closer to the N terminus and into residues known to contribute to the αBgt binding site (23). Truncation of mouse α1 after Pro^{211}, which is homologous with our truncation point in α7WS, did not disrupt the formation of a high affinity binding site for αBgt. In contrast, truncation of the mouse α1 subunit after Met^{207} (mouse α1 numbering) caused a loss of affinity for αBgt.

More extreme truncations of the ECD of α1 have been explored in attempts to bypass the difficulties presented by AChRs for structural studies. None, however, appears as successful in duplicating properties of full-length AChRs as the α7 ECD AChRs described here. For example, peptide sequences from the region around residues 170–200 of the α1 subunit have been used as potential mimics of the αBgt binding site for NMR and ligand-binding studies (62, 63). The affinity for the binding of αBgt, however, typically is three orders of magnitude less than with full-length AChRs (64). In addition, peptide models from the α1 subunit are incapable of oligomerization and do not show significant affinity for small ligands.

Three conclusions from our investigation are relevant to a strategy for obtaining α7 ECD AChRs for structural studies. First, the extracellular domain constitutes a stable, fully water-soluble AChR that quantitatively retains essential ligand-binding properties of the full-length AChR and eliminates confounding factors of detergent solubilization that hamper the crystallography of membrane proteins. Second, M1 in the α7M1 and α7EK constructs significantly enhances the yield of ECD AChRs compared with the yield from α7WS. Although membrane tethering of the AChR subunit proteins was essential for association of the ECD of the mouse muscle-type α1 subunit and the full-length δ subunit when expressed in COS cells (24), it was advantageous but not essential for assembly of α7WS AChR in oocytes. Third, the α7 ECD still can form an AChR even when a peptide spacer separates it from M1 and the adjacent membrane surface.

These findings suggest that a water-soluble α7 ECD AChR more likely will be produced in large amounts in two stages via a membrane-bound intermediate than directly from a water-soluble design of the ECD. The first stage is *in vivo* synthesis of a membrane-bound AChR that subsequently will be removed from its membrane tether by *in vitro* processing. The second stage is enzymatic removal of the membrane tether *in vitro*. α7EK demonstrates that an AChR substrate can be designed for specific proteolysis within a peptide spacer between the ECD and M1. Our attempts to separate an ECD AChR from the M1 domain of α7EK using EK, however, resulted in substantial nonspecific proteolysis. An alternative method that allows truncated α1 subunits to dimerize with full-length δ is substitution of M1 with a GPI moiety (24, 65). A GPI tether also leads to the expression of membrane-bound extracellular domains of chick α7 on the surface of oocytes (66). A GPI tether may be preferred at the stage of enzymatic processing, because the carbohydrate portion of the anchor at the C terminus of the protein can be separated from the more distal, membrane-embedded fatty acid portion with phosphatidylinositol-specific phospholipase C (67, 68). This enzyme is expected to eliminate the risk of nonspecific enzymatic proteolysis.

In addition to α7, we anticipate that ECD receptors of other members of the family of AChR subunits and other subunits of this entire superfamily of neurotransmitter-gated ion channels will mimic the structure and function of their respective full-length receptors. Demonstrations that ECD sequences are important in the assembly of both glycine receptors (69) and γ-aminobutyric acid$_A$ receptors (70) suggest that the ECD of other members of the superfamily also will fold and assemble autonomously. The ultimately successful design of an ECD AChR for high level expression may require other design modifications. Moreover, structural aspects of the gating and ion permeation functions of transmembrane domains will have to be explored with different strategies. A water-soluble, recombinantly generated ECD AChR, however, appears to be a promising foundation for structural studies of this superfamily of ion channels.

Acknowledgments—We thank Alexander Kuryatov for assistance with the use of α-toxin from *N. n. siamensis* and John C. Cooper and Lisa Burger for technical assistance.

REFERENCES

1. Lindstrom, J. (1996) in *Ion Channels* (Narahashi, T., ed) Vol. 4, pp. 377–450, Plenum Press, New York
2. Hucho, F., Tsetlin, V. I., and Machold, J. (1996) *Eur. J. Biochem.* **239,** 539–557
3. Karlin, A., and Akabas, M. H. (1995) *Neuron* **15,** 1231–1244
4. Chavez, R. A., and Hall, Z. W. (1992) *J. Cell Biol.* **116,** 385–393
5. Anand, R., Bason, L., Saedi, M. S., Gerzanich, V., Peng, X., and Lindstrom, J. (1993) *Biochemistry* **32,** 9975–9984
6. Galzi, J.-L., and Changeux, J.-P. (1994) *Curr. Opin. Struct. Biol.* **4,** 554–565
7. Tsigelny, I., Sugiyama, N., Sine, S. M., and Taylor, P. (1997) *Biophys. J.* **73,** 52–66
8. Corringer, P.-J., Galzi, J.-L., Eiselé, J.-L., Bertrand, S., Changeux, J.-P., and Bertrand, D. (1995) *J. Biol. Chem.* **270,** 11749–11752
9. Galzi, J.-L., Bertrand, D., Thiéry-Devillers, A., Revah, F., Bertrand, S., and Changeux, J.-P. (1991) *FEBS Lett.* **294,** 198–202
10. Beroukhim, R., and Unwin, N. (1995) *Neuron* **15,** 323–331
11. Unwin, N. (1993) *J. Mol. Biol.* **229,** 1101–1124
12. Unwin, N. (1995) *Nature* **373,** 37–43
13. Unwin, N. (1996) *J. Mol. Biol.* **257,** 586–596
14. Gu, Y., Camacho, P., Gardner, P., and Hall, Z. W. (1991) *Neuron* **6,** 879–887
15. Verrall, S., and Hall, Z. W. (1992) *Cell* **68,** 23–31
16. Yu, X. M., and Hall, Z. W. (1991) *Nature* **352,** 64–67
17. Kreienkamp, H.-J., Maeda, R. K., Sine, S. M., and Taylor, P. (1995) *Neuron* **14,** 1–20
18. Chavez, R. A., Maloof, J., Beeson, D., Newsom-Davis, J., and Hall, Z. W. (1992) *J. Biol. Chem.* **267,** 23023–23034
19. Sumikawa, K., and Nishizaki, T. (1994) *Mol. Brain Res.* **25,** 257–264
20. Sumikawa, K. (1992) *Mol. Brain Res.* **13,** 349–353
21. Hall, Z. (1992) *Trends Cell Biol.* **2,** 66–68
22. Yu, X. M., and Hall, Z. W. (1994) *Neuron* **13,** 247–255
23. Wang, Z.-Z., Hardy, S. F., and Hall, Z. W. (1996) *J. Biol. Chem.* **271,** 27575–27584
24. Wang, Z.-Z., Hardy, S. F., and Hall, Z. W. (1996) *J. Cell Biol.* **135,** 809–817
25. Wang, Z.-Z., Fuhrer, C., Shtrom, S., Sugiyama, J. E., Ferns, M. J., and Hall, Z. W. (1996) *Cold Spring Harbor Symp. Quant. Biol.* **61,** 363–371
26. García-Guzmán, M., Sala, F., Sala, S., Campos-Caro, A., and Criado, M. (1994) *Biochemistry* **33,** 15198–15203
27. Schoepfer, R., Conroy, W. G., Whiting, P., Gore, M., and Lindstrom, J. (1990) *Neuron* **5,** 35–48
28. Melton, D. A., Krieg, P. A., Rebagliati, M. R., Maniatis, T., Zinn, K., and Green, M. R. (1984) *Nucleic Acids Res.* **12,** 7035–7056

29. Gerzanich, V., Anand, R., and Lindstrom, J. (1994) *Mol. Pharmacol.* **45,** 212–220
30. LaVallie, E. R., Rehemtulla, A., Racie, L. A., DiBlasio, E. A., Ferenz, C., Grant, K. L., Light, A., and McCoy, J. M. (1993) *J. Biol. Chem.* **268,** 23311–23317
31. Anderson, L. E., Walsh, K. A., and Neurath, H. (1977) *Biochemistry* **16,** 3354–3360
32. Wilchek, M., Miron, T., and Kohn, J. (1984) *Methods Enzymol.* **104,** 3–55
33. Cheng, Y., and Prusoff, W. H. (1973) *Biochem. Pharmacol.* **22,** 3099–3108
34. Lazareno, S., and Birdsall, N. J. M. (1993) *Br. J. Pharmacol.* **109,** 1110–1119
35. Conroy, W. G., Saedi, M. S., and Lindstrom, J. (1990) *J. Biol. Chem.* **265,** 21642–21651
36. Karlsson, E., Arnberg, H., and Eaker, D. (1971) *Eur. J. Biochem.* **21,** 1–16
37. Anand, R., Peng, X., and Lindstrom, J. (1993) *FEBS Lett.* **327,** 241–246
38. Blount, P., Smith, M. M., and Merlie, J. P. (1990) *J. Cell Biol.* **111,** 2601–2611
39. Saedi, M. S., Conroy, W. G., and Lindstrom, J. (1991) *J. Cell Biol.* **112,** 1007–1015
40. Reynolds, J. A., and Karlin, A. (1978) *Biochemistry* **17,** 2035–2038
41. Palma, E., S., B., Binzoni, T., and Bertrand, D. (1996) *J. Physiol.* **491,** 151–161
42. Blount, P., and Merlie, J. P. (1989) *Neuron* **3,** 349–357
43. Tanford, C. (1961) *Physical Chemistry of Macromolecules*, pp. 379–382, John Wiley & Sons, New York
44. Cantor, C., and Schimmel, P. (1980) *Biophysical Chemistry*, Vol. 2, pp. 607–610, W. H. Freeman, San Francisco
45. Kuusine, A., Arvola, M., and Keinänen, K. (1995) *EMBO J.* **14,** 6327–6332
46. Arvola, M., and Keinänen, K. (1996) *J. Biol. Chem.* **271,** 15527–15532
47. de Vos, A. M., Ultsch, M., and Kossiakoff, A. A. (1992) *Science* **255,** 306–312
48. Somers, W., Ultsch, M., De Vos, A. M., and Kossiakoff, A. A. (1994) *Nature* **372,** 478–481
49. Muller, Y. A., Ultsch, M. H., Kelley, R. F., and de Vos, A. M. (1994) *Biochemistry* **33,** 10864–10870
50. Walter, M. R., Windsor, W. T., Nagabhushan, T. L., Lundell, D. J., Lunn, C. A., Zauodny, P. J., and Narula, S. K. (1995) *Nature* **376,** 230–235
51. Brown, J. H., Jardetzky, T. S., Gorga, J. C., Stern, L. J., Urban, R. G., Strominger, J. L., and Wiley, D. C. (1993) *Nature* **364,** 33–39
52. Hubbard, S. R., Wei, L., Ellis, L., and Hendrickson, W. A. (1994) *Nature* **372,** 746–754
53. Fields, B. A., Ober, B., Malchiodi, E. L., Lebedeva, M. I., Braden, B. C., Ysern, X., Kim, J. K., Shao, X., Ward, E. S., and Mariuzza, R. A. (1995) *Science* **270,** 1821–1824
54. Bentley, G. A., Boulot, G., Karjalainen, K., and Mariuzza, R. A. (1995) *Science* **267,** 1984–1987
55. Colman, P. M., Laver, W. G., Varghese, J. N., Baker, A. T., Tulloch, P. A., Air, G. M., and Webster, R. G. (1987) *Nature* **326,** 358–363
56. Wilson, I. A., Skehel, J. J., and Wiley, D. C. (1981) *Nature* **289,** 366–373
57. Milburn, M. V., Privé, G. G., Milligan, D. L., Scott, W. G., Yeh, J., Jancarik, J., Koshland, D. E., Jr., and Kim, S.-H. (1991) *Science* **254,** 1342–1347
58. Keller, S. H., Lindstrom, J., and Taylor, P. (1996) *J. Biol. Chem.* **271,** 22871–22877
59. Gelman, M. S., Chang, W., Thomas, D. Y., Bergeron, J. J. M., and Prives, J. M. (1995) *J. Biol. Chem.* **270,** 15085–15092
60. Vicente-Agulló, F., Rovira, J. C., Campos-Caro, A., Rodríguez-Ferrer, C., Ballesta, J. J., Sala, S., Sala, F., and Criado, M. (1996) *FEBS Lett.* **399,** 83–86
61. Tobimatsu, T., Fujita, Y., Fukuda, K., Tanaka, K., Mori, Y., Konno, T., Mishina, M., and Numa, S. (1987) *FEBS Lett.* **222,** 56–62
62. Basus, V. J., Song, G., and Hawrot, E. (1993) *Biochemistry* **32,** 12290–12298
63. Lentz, T. L. (1995) *Biochemistry* **34,** 1316–1322
64. Ohana, B., and Gershoni, J. M. (1990) *Biochemistry* **29,** 6409–6415
65. Englund, P. T. (1993) *Annu. Rev. Biochem.* **62,** 121–138
66. West, A. P., Jr., Bjorkman, P. J., Dougherty, D. A., and Lester, H. A. (1997) *J. Biol. Chem.* **272,** 25468–25473
67. Koke, J. A., Yang, M., Henner, D. J., Volwerk, J. J., and Griffith, O. H. (1991) *Protein Expr. Purif.* **2,** 51–58
68. Medof, M. E., Nagarajan, S., and Tykocinski, M. L. (1996) *FASEB J.* **10,** 574–586
69. Kuhse, J., Laube, B., Magalei, D., and Betz, H. (1993) *Neuron* **11,** 1049–1056
70. Hackam, A. S., Wang, T.-L., Guggino, W. B., and Cutting, G. R. (1997) *J. Biol. Chem.* **272,** 13750–13757